Par3/Bazooka promotes Notch pathway target gene activation

Jun Wu, Neeta Bala Tannan, Linh T. Vuong, Yildiz Koca, Giovanna M. Collu, and Marek Mlodzik

Affiliations

[1] Dept. of Cell, Developmental, and Regenerative Biology,

[2] Graduate School of Biomedical Sciences,

Icahn School of Medicine at Mount Sinai,

One Gustave L. Levy Place, New York, NY 10029.

Abstract

The conserved *bazooka (baz/par3*) gene acts as a key regulator of asymmetrical cell divisions across the animal kingdom. The associated Par3/Baz-Par6-aPKC protein complex is also well known for its conserved role in the establishment of apical/basal cell polarity in epithelial cells. Here we define a novel, positive function of Baz/Par3 in the Notch pathway. Using *Drosophila* wing and eye development, we demonstrate that Baz is needed for Notch-signaling activity and in general for correct transcriptional activation of Notch target genes. Baz appears to act independently of aPKC in these contexts, as knockdown of *aPKC* causes unrelated phenotypes. Our genetic *in vivo* data suggest that Baz acts the level of active NICD, the cleaved Notch intracellular domain, which upon pathway activation translocates to the nucleus and acts as a transcriptional co-activator. We also demonstrate a biochemical interaction between NICD and Baz. Taken together, our data define a novel role of the polarity protein Baz/Par3, as a positive and direct regulator of Notch signaling through its interaction with NICD.

Key Words:

Notch signaling, Par3, transcriptional target regulation, cell polarity, Drosophila, tissue patterning

Introduction

Cell polarity is a critical feature of most cell types and particularly so in epithelial cell sheets, which display a mandatory apical-basal (A/B) polarity that is required for their barrier function and vectorial secretion behavior. Similarly, stem cells often display polarized features, which are critical for stem cell maintenance and for progenitor cell fates. Here, when such polarized cells divide, the cell contents are asymmetrically inherited by the two daughter cells (e.g. rev. in [1, 2]). The mechanisms that govern the establishment and maintenance of cell polarity are evolutionarily conserved. The protein complexes that mediate polarization are also shared among distinct instances of cell polarization, for example between maintaining A/B polarity and asymmetric division of progenitor cells. Generally, the process is regulated by a set of protein complexes that were discovered genetically in *C. elegans* and *Drosophila* [3].

The conserved *par3* gene, known as *bazooka/baz* in *Drosophila*, was originally identified in *C. elegans*, where it acts as a key regulator of asymmetrical cell divisions in the very early embryo [4]. It generally acts together with Par6 and aPKC as a regulatory complex of many asymmetric cell divisions across the animal kingdom (reviewed in [1, 2]). This Par3/Baz-Par6-aPKC complex is also well known for its conserved role in the establishment of A/B polarity in epithelial cells [5]. Our interest in the A/B epithelial cell polarity proteins originates from the fact that several of these have also been linked to planar cell polarity (PCP), that is polarity within the epithelial sheet, orthogonal to the A/B axis [6], for example aPKC and Scribble [7, 8]. Both aPKC and Scribble can associate with core PCP factors, aPKC with Frizzled and Scribble with Van Gogh/Vang (Vangl in vertebrates), and they thus contribute to the stability and asymmetric segregation of the core PCP complexes and PCP establishment within an epithelial cell sheet [9]. To systematically examine whether additional A/B epithelial polarity factors can play a role in PCP establishment, we tested members of these protein families for PCP associated knockdown phenotypes during *Drosophila* wing development. Surprisingly when we examined

66 phenotypes of *baz/par3* knockdown in this context, we observed predominantly notching
67 features of the wing margin, a *Notch* mutant-like phenotype. Here we focus on investigating a
68 specific role for Baz in regulating Notch signaling.
69
70 *Notch (N)*, originally identified in *Drosophila* based on its haplo-insufficient, dominant wing-
71 notching phenotype [10-12], encodes a single-pass transmembrane receptor protein containing
72 EGF-like repeats in its extracellular domain [13] and a conserved intracellular domain (NICD)
73 that can translocate to the nucleus and function as transcriptional co-activator (reviewed in [14-
74 18]). Many subsequent studies demonstrated that the highly conserved Notch receptor family
75 plays important roles during almost all biological processes through cell-cell communication and
76 cellular signaling, controlling many target genes that can be either shared or context dependent
77 (reviewed in [14-19]. Misregulation of N-signaling is associated with many human diseases,
78 including cancer [19]. The Notch receptor is activated by the binding of ligands of the Delta (Dl)
79 or Serrate/Jagged (Ser) families from neighboring cells to trigger two cleavage events to release
80 NICD [15, 16, 20]. NICD can then translocate into the nucleus, where it interacts with
81 transcription factors of the Suppressor of Hairless (Su(H)/CSL) family, and co-activators,
82 including Mastermind, to activate target gene expression [16]. Notch signaling is subject to
83 many regulatory steps, ranging from receptor and ligand trafficking and protein stability
84 regulators to specific nuclear events at the transcriptional end of pathway activation, many of
85 which were initially identified in *Drosophila* [16].
86
87 Previous work has proposed an indirect role for Baz/Par3 in regulating Notch signaling outcome
88 during asymmetric cell divisions in *Drosophila*. During asymmetric cell division of the sensory
89 organ precursors (SOPs), specific protein complexes segregate to opposite sides of the cell
90 cortex in each dividing SOP cell, on one side the Baz/Par3-Par6-aPKC complex and on the
91 other the Gαi-Pins-Mud-Dlg-Numb-Neur complex. The two daughter cells that result from this

cell division adopt distinct cell fates due to the asymmetric distribution of the above complexes: with one daughter cell inheriting Baz/Par3-Par6-aPKC, and the other the Gαi-Pins-Mud-Dlg-Numb-Neur complex [2]. Notably, the asymmetric segregation of these complexes causes an asymmetric activation of Notch -signaling, as Numb is known to repress N-signaling by reducing Notch levels at the cell surface, either through internalization or inhibition of recycling [2]. As such, an indirect role of Baz/Par3 in the regulation of N-signaling has been proposed, acting through the promotion of the asymmetric segregation of the inhibitory Numb away from the Baz-containing daughter. However, due to this indirect role of Baz/Par3 in the pathway, this SOP model system is not suited to address a more direct role of Baz/Par3 in Notch-signaling.

Using *Drosophila* wing and eye development, we define a novel, direct and positive function of Baz/Par3 in Notch-signaling. We demonstrate that Baz is needed for full Notch-signaling activity and activation of Notch transcriptional target genes. Baz appears to act independently of aPKC in these contexts, as knockdown of *aPKC* causes PCP defects rather than Notch-associated phenotypes. Our data indicate that Baz may act the level of NICD, the cleaved active Notch fragment, which upon pathway activation translocates to the nucleus and acts as a transcriptional co-activator, or further downstream. We also demonstrate a biochemical interaction between NICD and Baz. Taken together, our data define a novel role of the polarity protein Baz/Par3, as a positive regulator of Notch signaling through its interaction with NICD.

Results

Reduction of *bazooka* causes phenotypes similar to *Notch* loss of function phenotypes

To assess potential functions of A/B-polarity factors in PCP, or other signaling pathways, we expressed two independent non-overlapping RNAi (IR) lines in the posterior compartment of developing wing discs with the *en-Gal4* driver (Figure 1 and Suppl. Figure S1). Surprisingly, with components of the Baz/Par3-Par6-aPKC complex we detected distinct outcomes. While knock-

118 down of aPKC showed classical PCP defects, as expected based on previous work [7], see also
119 below), both *baz-IR* lines caused wing margin loss in the posterior compartment (Figure 1A-C;
120 Baz protein levels were markedly reduced and barely detectable in the *baz-IR* expressing
121 domain: Figure 1E, and Suppl. Figure S1B-C). The loss of the wing margin is associated with a
122 reduction in Notch signaling or in effects on the Wg signaling pathway, as *wg* is a direct target of
123 Notch signaling along the dorsal/ventral compartment border (see also below); the gene name
124 *Notch* is associated with its haplo-insufficient wing notching phenotype (see above). Besides the
125 posterior compartment of the wing being slightly reduced, no other patterning defects were
126 observed in the *baz* knockdowns (Figure 1A-C). In contrast to *baz*, knockdown of either *aPKC*
127 or *par6* caused either cell lethality with loss of large areas of the posterior wing compartment at
128 25°C or 29°C. When *aPKC-IR* was expressed at reduced levels (driven at 18°C), causing a
129 milder knock-down, the posterior wing compartment was still markedly smaller (Figure 1D; note
130 that wing hairs were also often very short, Fig. 1D-D', orange arrows), but the wing margin
131 appeared largely normal (Figure 1B'-D'). PCP defects were also observed in the *aPKC-IR*
132 expressing domain (Figure 1D', green arrow indicating PCP hair orientation), consistent with the
133 previously identified role of aPKC in PCP [7]. *Par6-IR* mediated knock-down caused severe loss
134 of wing tissues even at 18°C, making it impossible to correlate these defects with a specific
135 cellular mechanism or signaling pathway (Suppl. Figure S1D-D'). Nevertheless, the wing
136 margin appeared relatively normal in areas where there was no tissue loss (Suppl. Figure S1D-
137 D', magenta arrows).
138
139 Taken together, knock down of *baz* caused a distinct loss-of-function (LOF) phenotype from
140 *aPKC* and *Par6*, affecting wing margin development. To confirm this effect, we also analyzed
141 wings containing mutant clones of baz^{4} or $baz^{815\text{-}8}$ alleles (Suppl. Figure S1A for allele
142 information). Consistent with the RNAi knock-downs, *baz* LOF clones also displayed wing
143 margin loss (Suppl. Figure S2A-C). On the notum, *baz* mutant LOF clones displayed loss of

144 sensory bristles (Suppl. Figure S2D-F), in accordance with previous work [21] confirming the
145 correct behavior of the *baz* alleles. Taken together with the RNAi phenotypes above, the *baz*
146 LOF clonal phenotypes in the wing suggest a potential role for Baz/Par3 in Notch-signaling.
147

148 ***Notch* and *baz* interact genetically**

149 To corroborate a relationship between *Notch* and *baz* phenotypes, we performed genetic
150 interaction analyses. In heterozygous conditions of the null allele N^{55e11}/+, approx. 30% of wings
151 displayed distal margin notching (near vein 3 and 4; Figure 2A, B, and F). We compared these
152 wings to double heterozygous combinations with the LOF *baz* alleles: baz^{4} and $baz^{815\text{-}8}$.
153 Strikingly, the double heterozygous animals displayed a marked enhancement of wing notching
154 with 68% and 79% of wing margin defects in N^{55e11}/baz^{4} and $N^{55e11}/baz^{815\text{-}8}$ allelic combinations,
155 respectively (Figure 2C-D, and F; see also Suppl. Figure S3). Moreover, in addition to the
156 enhanced distal wing notch phenotype, a novel defect appeared in the double heterozygous
157 animals with wing notching in the proximal region of the posterior compartment (Figure 2B', D'
158 and quantified in 2G; see also Suppl. Figure S3B'-C'). Whereas N^{55e11}/+ wings did not display
159 any notches in this proximal region (Figure 2B' and 2G), 100% of the double heterozygous
160 N^{55e11}/baz^{4} and $N^{55e11}/baz^{815\text{-}8}$ wings carried such margin defects (quantified in Figure 2G;
161 $p<0.0001$). The equivalent baz^{4}/+ and $baz^{815\text{-}6}$/+ heterozygous control wings did not display any
162 margin notching phenotypes (Figure 2E-E', also Suppl. Figure S3C-C'). These data suggest that
163 *Notch* and *baz* genetically interact during wing margin patterning in a synergistic manner.
164

165 We next asked whether interactions between *Notch* and *baz* are also detected in other tissues
166 and with a gain-of-function (GOF) N genotype. The specification of cell fates in the developing
167 eye requires Notch input at multiple steps, from early patterning of the presumptive eye field to
168 the specification of individual photoreceptor (R cell) and accessory cell fates. A classical
169 example of activation of N-signaling during eye patterning is the expression of active N

170 molecules under control of the *sevenless* (*sev*) enhancer (expressed in R3-4 and R1,6, and R7).
171 Elevated levels of Notch pathway activity can be induced by expressing N-terminally truncated
172 molecules that lack the inhibitory region in the extracellular domain that prevents γ-secretase-
173 mediated cleavage (NΔECD, [22]), or the intracellular domain itself, lacking any membrane
174 targeting sequence (NICD, [23]). Depending upon the strength of activation, elevated Notch
175 signaling induces the transformation of R3 to R4 or the R1/R6 photoreceptors to R7 [24, 25, 26,
176 27]. While the N-signaling requirement in R4 specification [24-26] cannot be used in this
177 context, as Baz is required to maintain high levels of Fz during PCP signaling and thus indirectly
178 affects R4 [7], the induction of R7 is a classical N-dependent cell fate and ectopic activation of N
179 causes the transformation of R1/R6 photoreceptors to R7 [27]. In the *sev-NICD* background a
180 large fraction of ommatidia display a multi-R7 phenotype (Figure 2H, and [27]), while removal of
181 one copy of the strong $baz^{815\text{-}8}$ allele in this background suppresses the GOF Notch effect
182 (Figure 2H). Taken together with the above genetic interactions with *N* LOF features, these
183 results suggest that Baz/Par3 is generally required for Notch signaling function in different
184 tissues and both in LOF and GOF scenarios.
185
186 **baz^{-} loss of function caused reduction of Notch target gene expression**
187 To test whether *baz-IR* affects Notch-signaling directly, we examined the expression of
188 endogenous Notch-signaling targets *wg* and *cut* [28, 29]. To monitor *wg* expression we
189 analyzed the expression of *wg-lacZ*, an enhancer trap insertion in the *wg* locus, which faithfully
190 reproduces *wg* expression patterns; and to monitor *cut* expression we used an antibody to Cut.
191 Knock-down of *baz* in the posterior compartment caused reduction of both *wg-lacZ* expression
192 and Cut protein levels, as compared to control levels in the anterior compartment (Figure 3A-
193 C"). Both *wg-lacZ* and Cut levels were significantly reduced in quantifications, by comparing
194 their intensity ratio between the anterior (control) and posterior (experimental) compartment

195 (Figure 3D-E). Since the reduction of *wg* and *cut* expression is detected at the third instar larval
196 stage in wing discs, before wing margin sensory development occurs at the pupal stages [30],
197 the *baz* effect on their expression precedes sensory cell differentiation and is thus clearly
198 separated in time from the known Baz function in asymmetric SOP cell division.
199
200 To confirm these results, we also examined the expression of the Notch response element
201 (NRE) reporter, *NRE-GFP* [31, 32]. In wing discs, *NRE-GFP* is expressed along the
202 dorsal/ventral compartment border in an indistinguishable pattern to endogenous Notch target
203 genes, as for example *wg* and *cut* [31] (Suppl. Figure S4A). Importantly, reduced expression of
204 *NRE-GFP* was observed in the posterior compartment in *enGal4>baz-IR(s)* wings (Suppl.
205 Figure S4B-C', and E), indicating that a reduction of *baz* directly correlated with reduced Notch-
206 signaling and target expression.
207
208 To corroborate these data and to test for a general effect of *baz* LOF on Notch signaling
209 outcomes in different tissues, we analyzed the expression of Notch targets in *baz* mutant clones.
210 Consistent with the *baz-IR* knockdown in wing discs, Cut expression levels were reduced in
211 $baz^{815\text{-}8}$ mutant cells (clones were positively labeled by RFP expression, Figure 4A-C, examples
212 highlighted with white arrows; quantified in Figure 4D). Next we tested for effects on Notch
213 signaling targets in eye discs. To test an independent Notch target gene, we asked whether
214 expression of *atonal* (*ato*), a N-signaling target during early eye patterning prior to R-cell
215 specification [33] also requires *baz* for its expression. Ato levels were reduced in $baz^{815\text{-}8}$ mutant
216 cells (orange arrows in Figure 4E-E", F-F", mutant clone marked by lack of GFP). Importantly,
217 apical-basal polarity as apparent in optical z-sections was normal in baz^{-} clones (Figure 4G-G";
218 note Patj as A/B marker being localized normally in $baz^{815\text{-}8}$ clones), whereas a reduction of Ato
219 expression was also easily detected in this optical plane (Figure 4D-F, orange arrows in E" and
220 F"; quantified in Figure 4H),

221

222 Taken together, these results are consistent with the notion that Baz functions as a positive
223 regulator within the Notch-signaling pathway, promoting the expression of Notch target genes.

224

225 **Baz affects Notch-signaling at the NICD level**

226 To mechanistically dissect Baz function in Notch signaling, we used N-terminal Notch
227 truncations in GOF assays to determine at what level within the pathway Baz was required.
228 First, we used NΔECD[22], which lacks the extracellular domain and is constitutively active
229 independent of ligand binding. As such, if NΔECD were affected by *baz* LOF, Baz would be
230 required downstream of the N-ligands and the subsequent extracellular cleavages of Notch, but
231 upstream of the γ-secretase-mediated cleavage [15, 20]. When NΔECD was clonally expressed
232 [34, 35] in larval wing discs, 43% of NΔECD clones induced the Notch target *wg* (Figure 5A, F;
233 as detected by Wg antibody). When *baz-IR(*s) were co-expressed in NΔECD clones, the
234 frequency of Wg expression, was reduced to 20% (*baz-IR*-1) and 27% (*baz-IR*-2) clones (Figure
235 5B, F). These data suggested that Baz was required at the level of the γ-secretase cleavage or
236 further downstream within the Notch-signaling pathway. Consistent with this hypothesis *baz-IR*
237 knock-down displayed no detectable effect on Notch protein levels at the membrane or cellular
238 distribution of Notch (Suppl. Figure S1E-F).

239

240 To further investigate the position of Baz within the Notch pathway, we tested the NICD
241 fragment, which is fully active and does not associate with the membrane or require any
242 cleavage and is thought to directly translocate to the nucleus to activate Notch-signaling target
243 genes as transcriptional co-activator [15, 16, 20, 23]. In control wing disc clones expressing
244 NICD, Wg expression was readily detected in 63% or 71% (with a control IR co-expression)
245 clones (Figure 5C-D, and G). In experimental clones, with *baz-IR*(s) being co-expressed with

246 NICD, the NICD effect was markedly suppressed: to 41% with *baz-IR*-1 and 32% with *baz-IR*-2,
247 respectively (Figure 5E, G). These data are consistent with the notion that Baz acts downstream
248 of membrane tethered Notch and that it is required for the ability of the NICD fragment to
249 activate Notch-signaling target gene expression.
250
251 The above *in vivo* studies suggested that Baz might either act in the nucleus or affect NICD
252 nuclear translocation. We therefore asked whether Baz and NICD physically interacted with
253 each other. This was tested biochemically via co-immunoprecipitation (co-IP) from S2 cell
254 samples that were co-transfected with HA-tagged NICD and either Baz-myc (full length Baz
255 tagged with myc) or myc-Hippo (Hpo, as negative control). Proteins extracted from S2 cell
256 samples were immunoprecipitated with anti-myc and analyzed by immunoblotting with anti-HA
257 antibody. NICD was readily co-immunoprecipitated with Baz-myc (Figure 6A), but not by the
258 Hpo control (Figure 6A-B; see figure legend for additional controls).
259
260 Taken together with the functional *in vivo* data, these results suggested that Baz and NICD were
261 associated in the same protein complex, and that the presence of Baz is required for normal
262 NICD function in signaling activation and Notch target gene expression.
263
264 **Discussion**
265 In this study we define a novel, direct, and positive role of the polarity protein Baz/Par3 in the
266 Notch pathway. This stands in contrast to its previously established role in Notch signaling
267 regulation during asymmetric SOP cell divisions, where Baz/Par3 affects N-signaling indirectly
268 by asymmetrically sequestering the Notch inhibitor Numb [2]. In the SOP scenario, the
269 Baz/Par3-Par6-aPKC protein complex localizes to one side within the dividing cell, and a Numb-
270 Neuralized containing complex localizes to the other side of the cell. As Numb inhibits Notch
271 signaling by regulating Notch-Sanpodo trafficking and thus reducing Notch levels at the cell

272 surface, this asymmetry causes Notch inhibition in the Numb containing daughter cell (reviewed
273 in [2]. In the SOP context, Baz/Par3 has been thus proposed to have a passive role in N-
274 signaling activation, via the asymmetric segregation of an inhibitor, Numb. Our data are
275 consistent with the notion that Baz/Par3 is also required positively for the Notch signaling
276 outcome and full transcriptional activation of Notch targets in *Drosophila* in many cell types.
277 Genetic epistasis studies and biochemical experiments indicate that Baz acts the level of
278 cleaved active Notch, NICD, or in parallel to it. Consistent with this notion Baz and NICD co-
279 immunoprecipitated, suggesting that Baz promotes Notch signaling at the level of NICD.
280

281 **A novel Baz/Par3 function independent of the A/B polarity complex**

282 Baz/Par3 is generally associated with Par6-aPKC at early to intermediate stages of A/B polarity
283 establishment, but later in mature epithelia it is not essential for their maintenance [36-38].
284 Indeed, the fact that we can recover *baz* LOF clones at all, whereas Par6 and aPKC are cell
285 lethal in null alleles, suggests that *baz* can behave differently to the 'core' A/B factors. In our
286 experimental set-up we observed no evidence for a Par6 or aPKC involvement in Notch
287 signaling. Our data suggest that Baz/Par3 regulates NICD independently of its role in the A/B
288 polarity complex. Similar to A/B polarity establishment, in the context of planar cell polarity
289 (PCP) patterning, Baz/Par3 functions together with aPKC to regulate Frizzled levels (and hence
290 the PCP outcomes) in the *Drosophila* eye [7], and thus, while Par6 could not be assayed in this
291 context, these data suggested that in PCP determination Baz is functioning with established A/B
292 polarity factors. As such, the discovery that in Notch signaling Baz/Par3 appears to function
293 completely independently of its partners in A/B establishment within the same tissue is
294 unexpected.
295

296 Par3 homologues have however been shown to act independently of the aPKC-Par6 complex in
297 several scenarios in mammalian cells, including Hippo/Yap signaling and during epithelial-

298 mesenchymal transition [39]. Par3 has even been suggested to act with Ku70 and Ku80 as part
299 of the DNA-dependent protein kinase complex to regulate double-strand breaks [40].
300
301 **Why was Baz/Par3 not identified earlier as a component of Notch signaling?**
302 The initial core Notch pathway genes were identified through classic genetic collections of
303 spontaneous mutants showing morphological defects in *Drosophila* and *C. elegans* [41-44].
304 Subsequent genetic screens and molecular studies have added many components of the Notch
305 pathway and many regulatory mechanisms that affect Notch signaling at all levels, ranging from
306 receptor and ligand trafficking and membrane stability and its membrane associated proteolytic
307 cleavages to nuclear co-factors and chromatin associated target gene regulation (reviewed in
308 [16-18]. In particular, many of the screens were performed using the notum Notch associated
309 phenotypes and score for asymmetric division-dependent SOP/bristle patterning defects. It has
310 thus been technically difficult, if not impossible, to separate potential additional Baz/Par3
311 involvements in Notch signaling. Similarly, classical loss-of-function screens in the *Drosophila*
312 embryo would have missed Baz/Par3 due to its initial requirement in epithelial polarization that
313 could have caused earlier lethality [45, 46], which obscures a potential role in subsequent
314 signaling events. Indirectly through our screen asking whether A/B polarity factors can also play
315 a role in PCP establishment or other pathways in the developing posterior wing disc
316 compartment we created a unique experimental scenario: first the posterior margin bristles are
317 not innervated SOPs and thus do not require N-signaling during asymmetric SOP divisions, and,
318 second, at this later stage of epithelial patterning Baz/Par3 is not required for maintenance of
319 apical/basal polarity. The combination of this thus allowed the identification of *baz* as a novel
320 factor that positively regulates Notch signaling outcomes.
321
322 **Baz acts at the NICD level affecting expression of N-signaling targets positively**

323 Genetic epistasis data, both in the wing and the eye, position the function of Baz/Par3 at the
324 level of NICD after it last cleavage, suggesting that Baz acts either in the nucleus together with
325 NICD or alternatively it might promote nuclear translocation or retention of NICD. The
326 biochemical immunoprecipitation results support the genetic data and are consistent with the
327 notion that Baz as a direct regulator of Notch signaling, acting at the level of NICD.
328 Interestingly, the human Baz/Par3 homologue, PARD3, has been suggested to act at a similar
329 level in the YAP/TAZ pathway. PARD3, which itself is found in the nucleus outside of the
330 junction-bound aPKC/Par6 complex, has been suggested to regulate TAZ phosphorylation and
331 its nuclear localization [39], as a scaffold for YAP-binding proteins. The Notch signaling pathway
332 is simpler than the pathway(s) that can activate YAP/TAZ proteins, as Notch acts as a
333 membrane-tethered transcriptional co-activator, without the complex cascade of kinase-
334 dependent steps as in YAP/TAZ regulation. Nonetheless, NICD is still regulated by
335 phosphorylation events, for example to limit prolonged pathway activity, through the action of
336 Mastermind and CycC:CDK8 [47]. It is possible that Baz/Par3 may also regulate NICD
337 phosphorylation and nuclear localization in a similar manner.
338
339 During Notch signaling, the associated DNA binding complex, centered around the Notch-
340 pathway dedicated DNA-binding factor CSL, Su(H) in *Drosophila*, switches from a repressor
341 complex to a transcriptional activator complex via NICD, which binds to Su(H) and also recruits
342 co-activators like Mastermind (Mam) [16]. The binding of NICD and Mam to Su(H)/CSL
343 displaces the repressing factors of the "repressor complex" and allows N-signaling target gene
344 transcription. Several factors have been identified that associate with Su(H)/CSL and NICD (see
345 reviews [16, 48]). Generally, the strength of activation of target gene expression depends on
346 NICD stability within the resulting activator complexes, which also contain histone
347 modifying/remodeling proteins, and accessibility of enhancers of any given target gene. As *baz*
348 mutations affect the levels of target gene expression and the Baz protein acts genetically at the

level of or in parallel to NICD, Baz/Par3 might be a factor participating in either scenario. N-signaling acts in many different contexts and can activate many distinct target genes, and as such the presence of context-determining factors will determine whether an enhancer is primed to react to a specific signal, which may result in a gene having different responses towards the same signals [49]. Our data suggest that Baz/Par3 acts rather generally on N-signaling target gene activation, as we see effects on Notch target expression in multiple tissues and on different target genes. The precise function of Baz/Par3 in the context of N-signaling target activation will require transcription specific assays to be explored in future studies.

358 **Materials and Methods**

359 ***Fly genetics and stocks.***

360 *w-IR* ($w^{JF01540}$, P{TRiP.JF01540}), *baz-IR-1* ($baz^{JF01078}$, P{TRiP.JF01078}), *baz-IR-2* ($baz^{JF01079}$,
361 P{TRiP.JF01079}), *aPKC-IR* ($aPKC^{JF01966}$, P{TRiP. JF01966}), *UAS-mCD8RFP,* baz^{4} *FRT9-2*
362 and $baz^{815\text{-}8}$ *FRT9-2* fly stocks were obtained from Bloomington Drosophila Stock Center.
363 $baz^{815\text{-}8}$ was recombined with FRT19A and then used for $baz^{815\text{-}8}$ mutant clonal analysis with
364 FRT19A MARCM stock (genotype: *w, tub-gal4, hs-flp, FRT19A; act-Gal4, UAS-mCD8RFP /*
365 *CyO*).

366 N^{55e11}/baz^{4} and $N^{55e11}/baz^{815\text{-}8}$ were generated by intercrossing via several crosses: *ubi-baz-*
367 *mcherry* [50] was recombined with Sb^{1} to generate *ubi-baz-mcherry* Sb^{1} flies. baz^{4} (or $baz^{815\text{-}8}$)
368 males with *ubi-baz-mcherry* Sb^{1} which rescued baz^{-} mutations (baz^{4} or $baz^{815\text{-}8}$; *ubi-baz-mcherry*
369 Sb^{1}/+) were crossed to $N^{55e11}/FM7$ females to generate N^{55e11}/baz^{4} or $N^{55e11}/baz^{815\text{-}8}$ females
370 (selected against Sb^{1} phenotype).

371

372 ***Immunohistochemistry and microscopy:***

373 The following antibodies were used in the study: guinea pig Anti-Baz 1:200 [51], rabbit anti-Dlg
374 1:3000-4000 [52], mouse anti-Wg 1:10-20 [53], mouse Anti-Cut 1:20-1:40 [54], rabbit anti-RFP
375 1:300 (Rockland Immunochemicals), rabbit anti-Galactosidase 1:2500 (Cappel). Mouse anti-
376 Cut and anti-Wg antibodies were obtained from Developmental Studies Hybridoma Bank at the
377 University of Iowa.

378 Adult wings and nota were imaged with conventional Zeiss Axioplan microscope. Immuno-
379 fluorescent samples were imaged with Leica TCS SP5 confocal microscope. Images were
380 projected and quantified with Fiji-Image J. Cut expression levels were measured in cell nuclei
381 marked by Hoechst staining. $baz^{815\text{-}8}$ mutant cells were outlined by RFP expression. Only first
382 row of $baz^{815\text{-}8}$ mutant cells right at D/V border were measured for “average Cut channel pixel
383 intensity” minus “average background pixel intensity outside Cut expression domain” (similar to

384 Figure S4D1) for each nucleus. Neighboring control A/P border cells were also measured for
385 "average Cut pixel intensity" minus "average background pixel intensity".
386
387 **Data visualization and Statistics:**
388 Data were plotted via Microsoft Excel and LibreOffice Calc. Fisher's exact test (two tailed) and
389 student t-test (unpaired) were used for statistical analyses to calculate probabilities of null
390 hypothesis with the web version of Graphpad.
391
392 **Cell Culture and co-immunoprecipitation**
393 NICD-HA pAc and myc-Hpo pAc were generous gifts from Ramanuj DasGupta and Duojia Pan
394 [55]. Baz-myc pAWM was generated from pAWM gateway vector (Drosophila Genomics
395 Resource Center) and *baz* pEntr 2B (a gift from Tony Harris).
396 1μg of NICD-HA pAc and Baz-myc pAWM or myc-Hpo pAc plasmids each were transfected into
397 *Drosophila* S2 cells in a 6-well plate with Qiagen Effectene. Cells were lysed one day after
398 transfection with IP buffer (20 mM HEPES pH 7.5, 100 mM NaCl, 0.05% Triton X100, 1 mM
399 EDTA, 5 mM DTT, 10mM NaVO4, 10% glycerol and protease inhibitor cocktail). The cell
400 lysates (1mg of total protein) were pre-cleared by incubating with protein A-sepharose beads
401 (Thermo Scientific 20333) for 1 hour at 4°C, followed by centrifugation to remove the beads.
402 Mouse anti-Myc antibody (sc-40, Santa Cruz technology) was used at 1/1000 dilution for
403 immunoprecipitation. The A-sepharose beads and antibody were incubated together to form
404 pre-immuno-precipitate complexes at 4°C for 1 hour, then incubated with lysates. Myc-tagged
405 protein and associated proteins were captured by protein A-sepharose/antibody complexes after
406 overnight incubation at 4°C. Samples were washed 4 times with IP buffer. Immunoprecipitates
407 were resuspended in SDS sample buffer, boiled for 5 min, separated by SDS-PAGE, and
408 transferred to nitrocellulose membrane for immunoblotting. The blots were incubated with
409 mouse anti-myc (Santa Cruz technology) or rat anti-HA (Roche) at 1:1000, subsequently with

410 anti-mouse or anti-rat IgG-HRP. Proteins were then detected by enhanced chemiluminescence
411 kit (Millipore).
412
413
414 **Acknowledgements**
415 We are grateful to Kwang-Wook Choi, Kyung-ok Cho, Ramanuj DasGupta, Tony Harris, Duojia
416 Pan, and Jennifer Zallen for Drosophila strains and antibodies, and to Cathie Pfleger for helpful
417 suggestions on the manuscript. We also thank the Bloomington Drosophila Stock Center for fly
418 strains, and the Developmental Studies Hybridoma Bank at University of Iowa for antibodies.
419 We would also like to thank the ISMMS Microscopy CoRE, where confocal microscopy was
420 performed and was in part supported by the Tisch Cancer Institute P30 CA196521 grant from
421 the NCI. This work was supported by National Institutes of Health grants R01 EY013256 and
422 R35 GM127103 and (to MM).
423

424 **References:**

425 1. Neumuller RA, Knoblich JA. Dividing cellular asymmetry: asymmetric cell division and its
426 implications for stem cells and cancer. Genes & development. 2009;23(23):2675-99. doi:
427 10.1101/gad.1850809. PubMed PMID: 19952104; PubMed Central PMCID: PMC2788323.

428 2. Schweisguth F. Asymmetric cell division in the Drosophila bristle lineage: from the
429 polarization of sensory organ precursor cells to Notch-mediated binary fate decision. Wiley
430 Interdiscip Rev Dev Biol. 2015;4(3):299-309. doi: 10.1002/wdev.175. PubMed PMID: 25619594;
431 PubMed Central PMCID: PMC4671255.

432 3. Goldstein B, Macara IG. The PAR proteins: fundamental players in animal cell
433 polarization. Developmental cell. 2007;13(5):609-22. doi: 10.1016/j.devcel.2007.10.007.
434 PubMed PMID: 17981131; PubMed Central PMCID: PMC2964935.

435 4. Etemad-Moghadam B, Guo S, Kemphues KJ. Asymmetrically distributed PAR-3 protein
436 contributes to cell polarity and spindle alignment in early C. elegans embryos. Cell.
437 1995;83(5):743-52. Epub 1995/12/01. doi: 10.1016/0092-8674(95)90187-6. PubMed PMID:
438 8521491.

439 5. Suzuki A, Ohno S. The PAR-aPKC system: lessons in polarity. Journal of cell science.
440 2006;119(Pt 6):979-87. doi: 10.1242/jcs.02898. PubMed PMID: 16525119.

441 6. Humphries AC, Mlodzik M. From instruction to output: Wnt/PCP signaling in
442 development and cancer. Curr Opin Cell Biol. 2018;51:110-6. doi: 10.1016/j.ceb.2017.12.005.
443 PubMed PMID: 29289896; PubMed Central PMCID: PMC5949250.

444 7. Djiane A, Yogev S, Mlodzik M. The apical determinants aPKC and dPatj regulate
445 Frizzled-dependent planar cell polarity in the Drosophila eye. Cell. 2005;121(4):621-31. PubMed
446 PMID: 15907474.

447 8. Courbard JR, Djiane A, Wu J, Mlodzik M. The apical/basal-polarity determinant Scribble
448 cooperates with the PCP core factor Stbm/Vang and functions as one of its effectors.
449 Developmental biology. 2009;333(1):67-77. Epub 2009/07/01. doi: S0012-1606(09)00993-2 [pii]
450 10.1016/j.ydbio.2009.06.024. PubMed PMID: 19563796.

451 9. Wang M, Marco P, Capra V, Kibar Z. Update on the Role of the Non-Canonical
452 Wnt/Planar Cell Polarity Pathway in Neural Tube Defects. Cells. 2019;8(10). doi:
453 10.3390/cells8101198. PubMed PMID: 31590237; PubMed Central PMCID: PMC6829399.

454 10. Mohr OL. Character changes caused by mutation of an entire region of a chromosome in
455 Drosophila. Genetics. 1919;4:275-82.

456 11. Southgate L, Sukalo M, Karountzos ASV, Taylor EJ, Collinson CS, Ruddy D, et al.
457 Haploinsufficiency of the NOTCH1 Receptor as a Cause of Adams-Oliver Syndrome With
458 Variable Cardiac Anomalies. Circ Cardiovasc Genet. 2015;8(4):572-81. doi:
459 10.1161/CIRCGENETICS.115.001086. PubMed PMID: 25963545; PubMed Central PMCID:
460 PMC4545518.

461 12. Guruharsha KG, Kankel MW, Artavanis-Tsakonas S. The Notch signalling system:
462 recent insights into the complexity of a conserved pathway. Nature reviews. 2012;13(9):654-66.
463 doi: 10.1038/nrg3272. PubMed PMID: 22868267; PubMed Central PMCID: PMC4369923.

464 13. Wharton KA, Johansen KM, Xu T, Artavanis-Tsakonas S. Nucleotide sequence from the
465 neurogenic locus notch implies a gene product that shares homology with proteins containing
466 EGF-like repeats. Cell. 1985;43(3 Pt 2):567-81. doi: 10.1016/0092-8674(85)90229-6. PubMed
467 PMID: 3935325.

468 14. Wilson A, Radtke F. Multiple functions of Notch signaling in self-renewing organs and
469 cancer. FEBS letters. 2006;580(12):2860-8. doi: 10.1016/j.febslet.2006.03.024. PubMed PMID:
470 16574107.

471 15. Andersson ER, Sandberg R, Lendahl U. Notch signaling: simplicity in design, versatility
472 in function. Development (Cambridge, England). 2011;138(17):3593-612. doi:
473 10.1242/dev.063610. PubMed PMID: 21828089.

474 16. Bray SJ. Notch signalling in context. Nat Rev Mol Cell Biol. 2016;17(11):722-35. doi:
475 10.1038/nrm.2016.94. PubMed PMID: 27507209.

476 17. Kopan R, Ilagan MX. The canonical Notch signaling pathway: unfolding the activation
477 mechanism. Cell. 2009;137(2):216-33. doi: 10.1016/j.cell.2009.03.045. PubMed PMID:
478 19379690; PubMed Central PMCID: PMC2827930.

479 18. Henrique D, Schweisguth F. Mechanisms of Notch signaling: a simple logic deployed in
480 time and space. Development (Cambridge, England). 2019;146(3):dev172148 doi: 10.1242/dev.
481 doi: 10.1242/dev.172148. PubMed PMID: 30709911.

482 19. Siebel C, Lendahl U. Notch Signaling in Development, Tissue Homeostasis, and
483 Disease. Physiol Rev. 2017;97(4):1235-94. doi: 10.1152/physrev.00005.2017. PubMed PMID:
484 28794168.

485 20. Struhl G, Greenwald I. Presenilin is required for activity and nuclear access of Notch in
486 Drosophila. Nature. 1999;398(6727):522-5. doi: 10.1038/19091. PubMed PMID: 10206646.

487 21. Roegiers F, Younger-Shepherd S, Jan LY, Jan YN. Bazooka is required for localization
488 of determinants and controlling proliferation in the sensory organ precursor cell lineage in
489 Drosophila. Proceedings of the National Academy of Sciences of the United States of America.
490 2001;98(25):14469-74. Epub 2001/12/06. doi: 10.1073/pnas.261555598. PubMed PMID:
491 11734647; PubMed Central PMCID: PMC64705.

492 22. Fortini ME, Rebay I, Caron LA, Artavanis-Tsakonas S. An activated Notch receptor
493 blocks cell-fate commitment in the developing Drosophila eye. Nature. 1993;365(6446):555-7.
494 Epub 1993/10/07. doi: 10.1038/365555a0. PubMed PMID: 8413612.

495 23. Kidd S, Lieber T, Young MW. Ligand-induced cleavage and regulation of nuclear entry of
496 Notch in Drosophila melanogaster embryos. Genes & development. 1998;12(23):3728-40. Epub
497 1998/12/16. doi: 10.1101/gad.12.23.3728. PubMed PMID: 9851979; PubMed Central PMCID:
498 PMCPMC317253.

499 24. Cooper MT, Bray SJ. Frizzled regulation of Notch signalling polarizes cell fate in the
500 Drosophila eye. Nature. 1999;397(6719):526-30. doi: 10.1038/17395.

501 25. Fanto M, Mlodzik M. Asymmetric Notch activation specifies photoreceptors R3 and R4
502 and planar polarity in the Drosophila eye. Nature. 1999;397(6719):523-6. Epub 1999/02/24. doi:
503 10.1038/17389. PubMed PMID: 10028968.

504 26. Tomlinson A, Struhl G. Decoding vectorial information from a gradient: sequential roles
505 of the receptors Frizzled and Notch in establishing planar polarity in the Drosophila eye.
506 Development (Cambridge, England). 1999;126(24):5725-38.

507 27. Tomlinson A, Struhl G. Delta/Notch and Boss/Sevenless signals act combinatorially to
508 specify the Drosophila R7 photoreceptor. Molecular cell. 2001;7(3):487-95. doi: 10.1016/S1097-
509 2765(01)00196-4.

510 28. Neumann CJ, Cohen SM. A hierarchy of cross-regulation involving Notch, wingless,
511 vestigial and cut organizes the dorsal/ventral axis of the Drosophila wing. Development
512 (Cambridge, England). 1996;122(11):3477-85.

513 29. Micchelli CA, Rulifson EJ, Blair SS. The function and regulation of cut expression on the
514 wing margin of Drosophila: Notch, Wingless and a dominant negative role for Delta and Serrate.
515 Development (Cambridge, England). 1997;124(8):1485-95. Epub 1997/04/01. PubMed PMID:
516 9108365.

517 30. Jack J, Dorsett D, Delotto Y, Liu S. Expression of the cut locus in the Drosophila wing
518 margin is required for cell type specification and is regulated by a distant enhancer.
519 Development (Cambridge, England). 1991;113(3):735-47. PubMed PMID: 1821846.

520 31. Saj A, Arziman Z, Stempfle D, van Belle W, Sauder U, Horn T, et al. A combined ex vivo
521 and in vivo RNAi screen for notch regulators in Drosophila reveals an extensive notch
522 interaction network. Developmental cell. 2010;18(5):862-76. doi: 10.1016/j.devcel.2010.03.013.
523 PubMed PMID: 20493818.

524 32. Furriols M, Bray S. A model Notch response element detects Suppressor of Hairless-
525 dependent molecular switch. Curr Biol. 2001;11(1):60-4. Epub 2001/02/13. doi: 10.1016/s0960-
526 9822(00)00044-0. PubMed PMID: 11166182.

527 33. Freeman ABaM. Notch signalling and the initiation of neural development in the
528 Drosophila eye. Development (Cambridge, England). 2001;128:3889-98.

529 34. Ito K, Awano W, Suzuki K, Hiromi Y, Yamamoto D. The Drosophila mushroom body is a
530 quadruple structure of clonal units each of which contains a virtually identical set of neurones
531 and glial cells. Development (Cambridge, England). 1997;124(4):761-71.

532 35. Pignoni F, Zipursky SL. Induction of Drosophila eye development by decapentaplegic.
533 Development (Cambridge, England). 1997;124(2):271-8.

534 36. Morais-de-Sa E, Mirouse V, St Johnston D. aPKC phosphorylation of Bazooka defines
535 the apical/lateral border in Drosophila epithelial cells. Cell. 2010;141(3):509-23. doi:
536 10.1016/j.cell.2010.02.040. PubMed PMID: 20434988; PubMed Central PMCID: PMC2885938.

537 37. St Johnston D, Sanson B. Epithelial polarity and morphogenesis. Curr Opin Cell Biol.
538 2011;23(5):540-6. doi: 10.1016/j.ceb.2011.07.005. PubMed PMID: 21807488.

539 38. Tepass U. The apical polarity protein network in Drosophila epithelial cells: regulation of
540 polarity, junctions, morphogenesis, cell growth, and survival. Annual review of cell and

541 developmental biology. 2012;28:655-85. doi: 10.1146/annurev-cellbio-092910-154033. PubMed
542 PMID: 22881460.

543 39. Zhang P, Wang S, Wang S, Qiao J, Zhang L, Zhang Z, et al. Dual function of
544 partitioning-defective 3 in the regulation of YAP phosphorylation and activation. Cell Discov.
545 2016;2:16021. Epub 2016/07/28. doi: 10.1038/celldisc.2016.21. PubMed PMID: 27462467;
546 PubMed Central PMCID: PMCPMC4932730.

547 40. Fang L, Wang Y, Du D, Yang G, Tak Kwok T, Kai Kong S, et al. Cell polarity protein
548 Par3 complexes with DNA-PK via Ku70 and regulates DNA double-strand break repair. Cell
549 research. 2007;17(2):100-16. Epub 2007/02/09. doi: 10.1038/sj.cr.7310145. PubMed PMID:
550 17287830.

551 41. Lindsley DL, Zimm GG. The Genome of Drosophila melanogaster.1992.

552 42. Greenwald I. lin-12, a nematode homeotic gene, is homologous to a set of mammalian
553 proteins that includes epidermal growth factor. Cell. 1985;43(3 Pt 2):583-90. Epub 1985/12/01.
554 doi: 10.1016/0092-8674(85)90230-2. PubMed PMID: 3000611.

555 43. Fleming RJ, Scottgale TN, Diederich RJ, Artavanis-Tsakonas S. The gene Serrate
556 encodes a putative EGF-like transmembrane protein essential for proper ectodermal
557 development in Drosophila melanogaster. Genes & development. 1990;4(12A):2188-201. Epub
558 1990/12/01. doi: 10.1101/gad.4.12a.2188. PubMed PMID: 2125287.

559 44. Kopczynski CC, Alton AK, Fechtel K, Kooh PJ, Muskavitch MA. Delta, a Drosophila
560 neurogenic gene, is transcriptionally complex and encodes a protein related to blood
561 coagulation factors and epidermal growth factor of vertebrates. Genes & development.
562 1988;2(12B):1723-35. Epub 1988/12/01. doi: 10.1101/gad.2.12b.1723. PubMed PMID:
563 3149249.

564 45. Muller HA, Wieschaus E. armadillo, bazooka, and stardust are critical for early stages in
565 formation of the zonula adherens and maintenance of the polarized blastoderm epithelium in
566 Drosophila. The Journal of cell biology. 1996;134(1):149-63. doi: 10.1083/jcb.134.1.149.
567 PubMed PMID: 8698811; PubMed Central PMCID: PMC2120925.

568 46. Harris TJ, Peifer M. Adherens junction-dependent and -independent steps in the
569 establishment of epithelial cell polarity in Drosophila. The Journal of cell biology.
570 2004;167(1):135-47. PubMed PMID: 15479740.

571 47. Fryer CJ, White JB, Jones KA. Mastermind recruits CycC:CDK8 to phosphorylate the
572 Notch ICD and coordinate activation with turnover. Molecular cell. 2004;16(4):509-20. doi:
573 10.1016/j.molcel.2004.10.014. PubMed PMID: 15546612.

574 48. Borggrefe T, Oswald F. The Notch signaling pathway: transcriptional regulation at Notch
575 target genes. Cell Mol Life Sci. 2009;66(10):1631-46. doi: 10.1007/s00018-009-8668-7. PubMed
576 PMID: 19165418.

577 49. Housden BE, Terriente-Felix A, Bray SJ. Context-dependent enhancer selection confers
578 alternate modes of notch regulation on argos. Molecular and cellular biology. 2014;34(4):664-
579 72. Epub 2013/12/11. doi: 10.1128/mcb.01045-13. PubMed PMID: 24324007; PubMed Central
580 PMCID: PMCPMC3911485.

581 50. Bosveld F, Bonnet I, Guirao B, Tlili S, Wang Z, Petitalot A, et al. Mechanical control of
582 morphogenesis by Fat/Dachsous/Four-jointed planar cell polarity pathway. Science (New York,
583 NY. 2012;336(6082):724-7. doi: 10.1126/science.1221071. PubMed PMID: 22499807.

584 51. Blankenship JT, Fuller MT, Zallen JA. The Drosophila homolog of the Exo84 exocyst
585 subunit promotes apical epithelial identity. Journal of cell science. 2007;120(Pt 17):3099-110.
586 doi: 10.1242/jcs.004770. PubMed PMID: 17698923.

587 52. Izaddoost S, Nam SC, Bhat MA, Bellen HJ, Choi KW. Drosophila Crumbs is a positional
588 cue in photoreceptor adherens junctions and rhabdomeres. Nature. 2002;416(6877):178-83.
589 doi: 10.1038/nature720. PubMed PMID: 11850624.

590 53. Brook WJ, Cohen SM. Antagonistic interactions between wingless and decapentaplegic
591 responsible for dorsal-ventral pattern in the Drosophila Leg. Science (New York, NY.
592 1996;273(5280):1373-7. Epub 1996/09/06. PubMed PMID: 8703069.

593 54. Blochlinger K, Bodmer R, Jan LY, Jan YN. Patterns of expression of cut, a protein
594 required for external sensory organ development in wild-type and cut mutant Drosophila
595 embryos. Genes & development. 1990;4(8):1322-31. doi: 10.1101/gad.4.8.1322. PubMed
596 PMID: 1977661.

597 55. Wu S, Huang J, Dong J, Pan D. hippo Encodes a Ste-20 Family Protein Kinase that
598 Restricts Cell Proliferation and Promotes Apoptosis in Conjunction with salvador and warts.
599 Cell. 2003;114(4):445-56. doi: 10.1016/s0092-8674(03)00549-x.

600 56. Blair SS. Genetic mosaic techniques for studying Drosophila development. Development
601 (Cambridge, England). 2003;130(21):5065-72. PubMed PMID: 12975340.

602

603

604 **Figures**

605 **Figure 1**. Reduction of *bazooka/baz function* causes wing margin bristle loss.

606 (A-D) Overview and high magnification view (A'-D') of wings of the indicated genotypes.

607 (A, A') Wild-type wing; note the associated margin bristles in high magnification of area of

608 posterior wing margin (A'). Cellular hairs point towards the distal margin (green arrow).

609 (B, B') *enGal4, UAS-baz-IR-1* wing, with *baz* knock-down in the posterior compartment; note

610 loss of margin bristles (magenta arrows). Cellular hair orientation was not significantly affected.

611 (Genotype: *UAS-dcr2; enGal4, UAS-RFP, NRE-GFP / UAS-Baz-IR-1 at 29°C*)

612 (C, C') *enGal4, UAS-baz-IR2* wing (independent RNAi, see Fig. S1), displaying very similar loss

613 of margin bristles phenotype with hair orientation not significantly affected. (Genotype: *UAS-*

614 *dcr2; enGal4, UAS-RFP, NRE-GFP / UAS-Baz-IR-2 at 29°C*)

615 (D, D') *enGal4, UAS-aPKC-IR* wing, displaying largely normal margin bristle development. Note

616 wing size reduction in posterior compartment with some areas displaying abnormally short wing

617 hairs (orange arrow) and other areas with cellular hair orientation defects, suggesting that

618 reduction of aPKC affected several aspects of wing development, yet had no effect on margin

619 bristle development (Genotype: *enGal4* /+; *UAS-aPKC-IR (aPKC^{JF01966})* /+ at 19°C)

620 (E-E") RNAi-based knock down of Baz protein in posterior compartment. All panels are showing

621 max-projections of a stack of confocal images (~40μm to cover the apical surface of all of the

622 wing pouch area), including composite (E) and individual channels. Anti-Dlg (Discs large, green

623 and E') staining, serves as positive control to outline cells in both anterior (labeled "A") and

624 posterior compartments (labeled "P"). Anti-Baz (magenta) levels were markedly reduced in the

625 posterior *baz-IR* expressing compartment, suggesting an effective knock-down via the *baz* RNAi

626 transgene. (Genotype: *dcr2; enGal4/+; /UAS-baz-IR-2 29°C*).

627

628 **Figure 2.** *Notch* and *baz* interact genetically during wing margin patterning.

629 (A-B) Heterozygous N^{55e11}/+ wings display wing margin notching phenotypes; approx. 2/3 of *N*/+
630 wings are normal with no margin loss (example in A), while 1/3 displayed distal margin notches
631 (B, arrow). Proximal posterior wing margin was always normal (boxed area in B, and B') in all
632 animals. Quantified in panels (F) and (G).
633 (C-D) N^{55e11}/baz^{815-8} double heterozygous wings. Note increased margin notching in distal area
634 (D, arrows) and proximal-posterior wing margin in all wings (C, D and D', arrows). (D') Higher
635 magnification of boxed area in D. Quantified in panels (F) and (G).
636 (E) baz^{815-8}/+ single heterozygous wings show no margin notching, neither distally nor in the
637 proximal-posterior region (E', boxed area from E shown at higher magnification).
638 (F) Quantification of distal wing margin phenotypes as percentage of wings containing notching
639 (genotypes as indicated). Note that N^{55e11}/baz^{4} and N^{55e11}/baz^{815-8} flies show enhanced defects
640 (higher percentage) of margin notching as compared to N^{55e11}/+ alone (p=0.0062 and p=0.0033,
641 respectively (Fisher's exact test). The control baz^{4}/+ and baz^{815-8}/+ single heterozygous flies
642 have no wing margin phenotypes.
643 (G) Quantification of proximal wing margin phenotypes (posterior compartment) as percentage
644 of wings with margin loss (genotypes as indicated). 100% of N^{55e11}/baz^{4} and N^{55e11}/baz^{815-8} had
645 proximal wing margin notches. N^{55e11}/+, baz^{4}/+ and baz^{815-8}/+ heterozygous flies have no
646 proximal wing margin defects. p<0.0001 (Fisher's exact test) for phenotypic differences between
647 both double heterozygous combinations and N^{55e11}/+.
648 (H) baz^{815-8}/+ heterozygosity suppresses the *sev-NICD*/+ gain-of-function eye phenotype. *sev-*
649 *NICD* induces several phenotypes, and most prominently a transformation of the R1/R6 outer
650 photoreceptors to R7s, which results in ommatidia classified as 4:3 (4 outer R-cells and 3 R7s)
651 or 5:2 (5 outer R-cells and 2 R7s), in contrast to *wt*, which has a 6:1 appearance (6 outer R-cells
652 and 1 R7). Note that heterozygosity of baz suppresses the effect of sev-NICD and reverts the
653 ommatidial appearance partially towards 6:1 (the *wt* appearance).
654

655 **Figure 3.** Notch target gene expression is affected in *baz* mutant cells.

656 (A-C") Confocal images of third instar wing discs with expression of Notch target genes: *wg-lacZ*
657 (detected with anti-βGal, red; monochrome in A', B', and C') and *cut* (anti-Cut, blue;
658 monochrome in A", B", and C") are shown in wild type (A-A"), *baz-IR-1* (B-B"), and *baz-IR-2* (C-
659 C") genotypes. *wg-LacZ* and Cut expression are both reduced within the *enGal4>IR* expression
660 domain (posterior compartment, marked by GFP in green). Genotypes: (A) *UAS-dcr2; enGal4,*
661 *UAS-GFP / wg-lacZ*. (B) *UAS-dcr2; enGal4, UAS-GFP / wg-lacZ; baz-IR-1* (*BL31522)/+*. (C)
662 *UAS-dcr2; enGal4, UAS-GFP / baz-IR-2 (BL31523)/+* (all at 29°C).

663 (D) Quantification of intensity ratio of Cut expression between anterior and posterior
664 compartments (see Materials and Methods for details). Note reduction with both independent
665 *baz-IR* transgenes: *p*-values 0.0003 and 0.0001 (student t-test), respectively. (E) Quantification
666 of intensity ratio of *wg-lacZ* expression (anti-βgal staining) between anterior and posterior
667 compartments (*p*-values 0.002, and 0.001, respectively).

668

669 **Figure 4**. (A-A") Confocal optical section of $baz^{815\text{-}8}$ wing disc clone (positively labeled by co-
670 expression of RFP), and (B-B") cross-section of same $baz^{815\text{-}8}$ clone at position indicated by
671 yellow line in (A). Cut expression is reduced in *baz* mutant cells. Yellow line traverses Cut
672 expression domain in two regions indicated by white and blue arrows. Cut levels in $baz^{815\text{-}8}$
673 mutant cells (white arrow) are reduced, as compared to heterozygous control cells (blue
674 arrows). Genotype: *w, tub-gal4, hs-flp, FRT19A/* $baz^{815\text{-}8}$ *FRT19A; act-Gal4, UAS-mCD8RFP /+.*
675 (C-C"') Projection of 3 optical sections at clonal region in D/V border cells, showing Cut (green,
676 monochrome in C"') expressing cells. Cut is normally expressed in two rows, each flanking the
677 D/V-boundary on the respective side. Note that $baz^{815\text{-}8}$ mutant cells (RFP+, in red) in the cells
678 abutting the D/V-boundary express Cut at markedly reduced levels or not at all (examples
679 highlighted by white arrows), nuclei are marked by Hoechst (blue in C, or turquoise in C"). (D)

680 Quantification of Cut expression levels of D/V border cells (measured by average pixel intensity
681 for each cell, see Materials and Methods for details), plotted to compare Cut levels between
682 control and *baz*$^{815\text{-}8}$ mutant cells. Note higher Cut expression in neighboring wild-type cells, as
683 compared to *baz*$^{815\text{-}8}$ mutant cells.
684 (E-E") Ato expression at and near the morphogenetic furrow (MF) in eye imaginal discs.
685 containing *baz*$^{815\text{-}8}$ mutant clone (marked by absence of GFP expression, red, highlighted by
686 white outlines). Note markedly reduced Ato expression (green) in many mutant cells (orange
687 arrows in E', E"), although some remained unaffected (E' and E", white arrow). All cells,
688 including those with low Ato expression levels, stained equally well with nuclear marker
689 (Hoechst, blue in E, magenta in E'). (F-G") Two z-section views of *baz*$^{815\text{-}8}$ mutant clone in
690 furrow region, with (F) scanned through the middle of Ato expression stripe. Note that many
691 *baz*$^{815\text{-}8}$ mutant cells displayed markedly reduced or lost Ato expression (orange arrows in F")
692 with Hoechst (Hoechst, blue in F,G and magenta in F',G') staining serving as control. (G) z-
693 scan through posterior region of Ato expression stripe, where scan-plane intersected with the
694 apical domain (due to tissue shape of the MF and pseudo-stratified epithelium of imaginal disc)
695 reflecting junctional marker Patj (blue in G, magenta in G"). Note that apical junctional region
696 remains intact in *baz*$^{815\text{-}8}$ mutant cells, indicating that apical-basal polarity was not affected.
697 Genotype: *baz*$^{815\text{-}8}$ *FRT9-2/hsflp ubi-GFP FRT9-2*. (H) Quantification of Ato expressing cells in
698 *baz*$^{815\text{-}}$ clones and neighboring wild-type control cells revealed a decrease in Ato positive cells in
699 *baz*$^{815\text{-}}$ mutant clone vs wild-type control. Distributions were significantly different based on
700 Fisher's exact test.
701
702 **Figure 5.** Baz acts at the level of NICD or further downstream within Notch-signaling pathway.
703 (A-A') NΔECD expressed via flip-out clones; it can induce ectopic Wg expression within wing
704 blade precursor cells (Wg in red, monochrome in A'; clones labeled by co-expression of GFP in
705 A). Endogenous Wg expression stripe at DV-boundary serves as control (blue arrow in A') here

706 and in other genotypes, clones overlapping with endogenous Wg stripe were not scored in
707 quantification. Arrowheads mark examples of NΔECD expressing clones (white in A, red in A'),
708 many of which induce Wg expression. Only clones in the wing pouch proper (pouch outlined by
709 green lines) were scored for Wg expression. Genotype: *hsflp/UAS-dcr2; act>y*$^{+}$*>Gal4, UAS-*
710 *GFP/+; UAS-NΔECD /+.*

711 (B-B') Clonal co-expression of NΔECD with *baz-IR-2* markedly reduced the number of Wg
712 expressing clones (Wg in red, monochrome in B'; clones labeled by co-expression of GFP).
713 Arrowheads mark examples of NΔECD expressing clones (white in B, red in B'); note reduction
714 in such clones expressing Wg (compare to A,A') Genotype: *hsflp/ UAS-dcr2; act5c>y*$^{+}$*>Gal4,*
715 *UAS-GFP/+; UAS-NΔECD /baz-IR-2*.

716 (C-C') NICD expressing clones induce ectopic Wg expression with high frequency (Wg in red,
717 monochrome in C'; clones labeled by GFP). Arrowheads highlight examples of NICD expressing
718 clones (white in C, red in C'). Genotype: *hsflp/UAS-dcr2: act5c>y*$^{+}$*>Gal4, UAS-GFP/+; UAS-*
719 *NICD /+.*

720 (D-D') *IR* control (*white*/*w-IR*) co-expressed in NICD in clones. Ectopic Wg expression was
721 induced at similar frequencies to NICD alone (Wg in red, monochrome in D'; clones labeled by
722 GFP). Arrowheads highlight examples of NICD expressing clones (white in D, red in D').
723 Genotype: *hsflp/UAS-dcr2: act5c>y*$^{+}$*>Gal4, UAS-GFP/ UAS-NICD /*+; *w-IR/*+.

724 (E-E') Clonal co-expression of NICD with *baz-IR-2* markedly reduced the number of Wg
725 expressing clones (Wg in red, monochrome in E'; clones labeled by GFP). Arrowheads highlight
726 examples of NICD expressing clones (white in E, red in E'). Genotype: *hsflp/ UAS-dcr2;*
727 *act5c>y*$^{+}$*>Gal4, UAS-GFP/UAS-NICD; baz-IR-2/+.*

728 (F) Quantification of NΔECD clones with induced Wg expression with or without *baz-IR(s)*. The
729 frequency of Wg activation in *>NΔECD* clones was markedly reduced by the presence of *baz-*

730 *IR-1 or baz-IR-2* (p=0.0008 or p=0.011, respectively). Only clones inside wing pouch region
731 were counted, due to *wg* expression being regulated by other pathways outside pouch region.
732 (G) Quantification of NICD expressing clones with induced Wg expression with genotypes as
733 indicated (with *w-IR* (control), *baz-IR-1*, and *baz-IR-2*). Wg expression frequency in NICD clones
734 was markedly reduced when *baz-IR-1 or baz-IR-2* were co-expressed (both p<0.001 comparing
735 to NICD alone or NICD with *w-IR*; as calculated by Fisher's exact test).
736
737 **Figure 6.** Baz is detected in the same protein complex as NICD.
738 Baz (myc-tagged) or myc-Hippo (Hpo, negative control) and HA-tagged NICD were co-
739 transfected into S2 cells. Lysates of transfected cells were immnunoprecipitated (IP-ed) with
740 anti-myc antibody.
741 (A) Upper panel: Western blot showing NICD-HA detected in lysates of cells co-transfected with
742 myc-Hpo or Baz-myc. Lower panel: Anti-myc co-IP experiments, note NICD-HA was co-IPed
743 with Baz-myc, whereas it was not IP-ed by myc-Hpo (specificity control).
744 (B) Both Baz-myc and myc-Hpo were efficiently pulled down with anti-Myc in cell lysates co-
745 transfected with NICD-HA.

746 **Figure 1:**

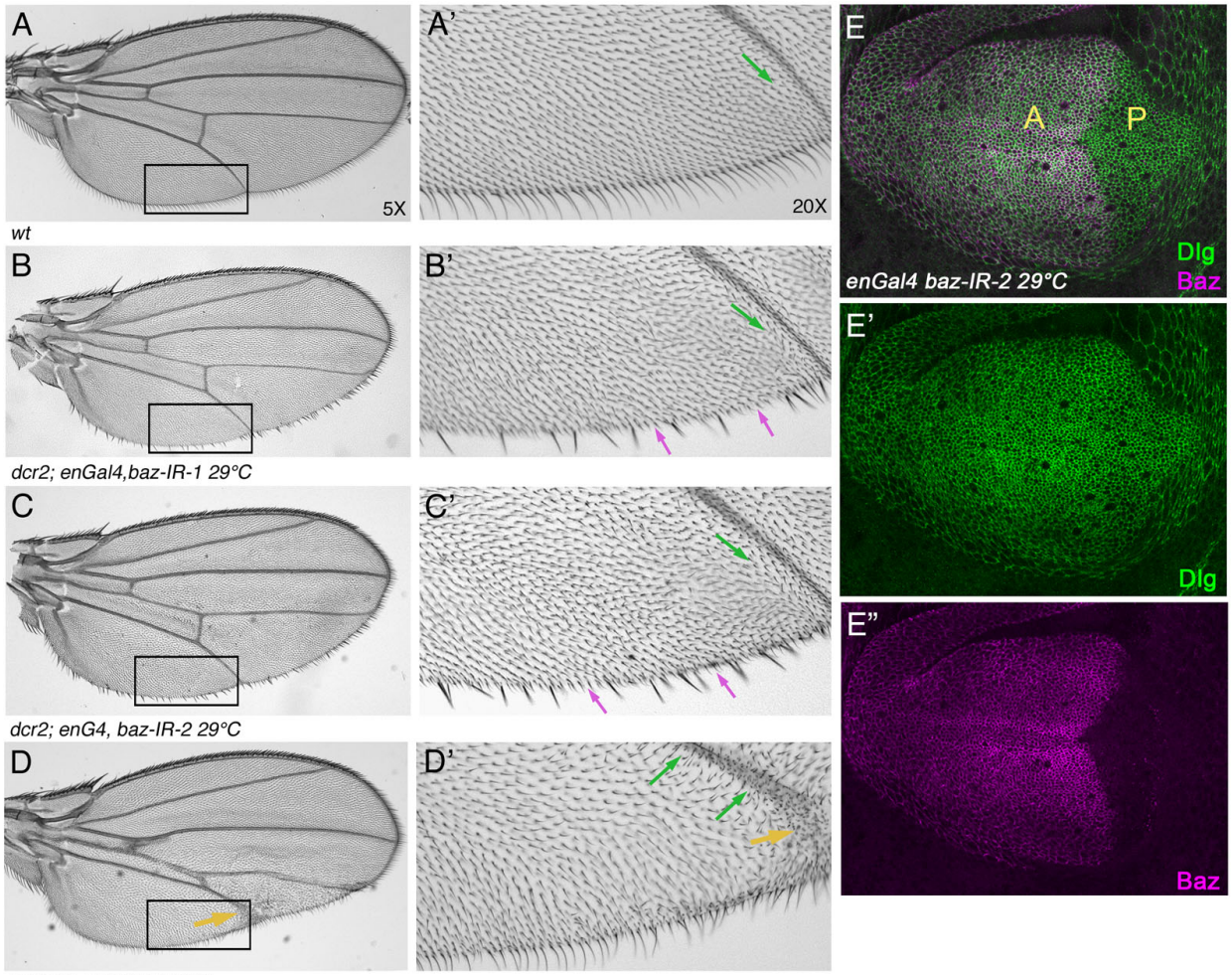

747

748

749

750 **Figure 2:**

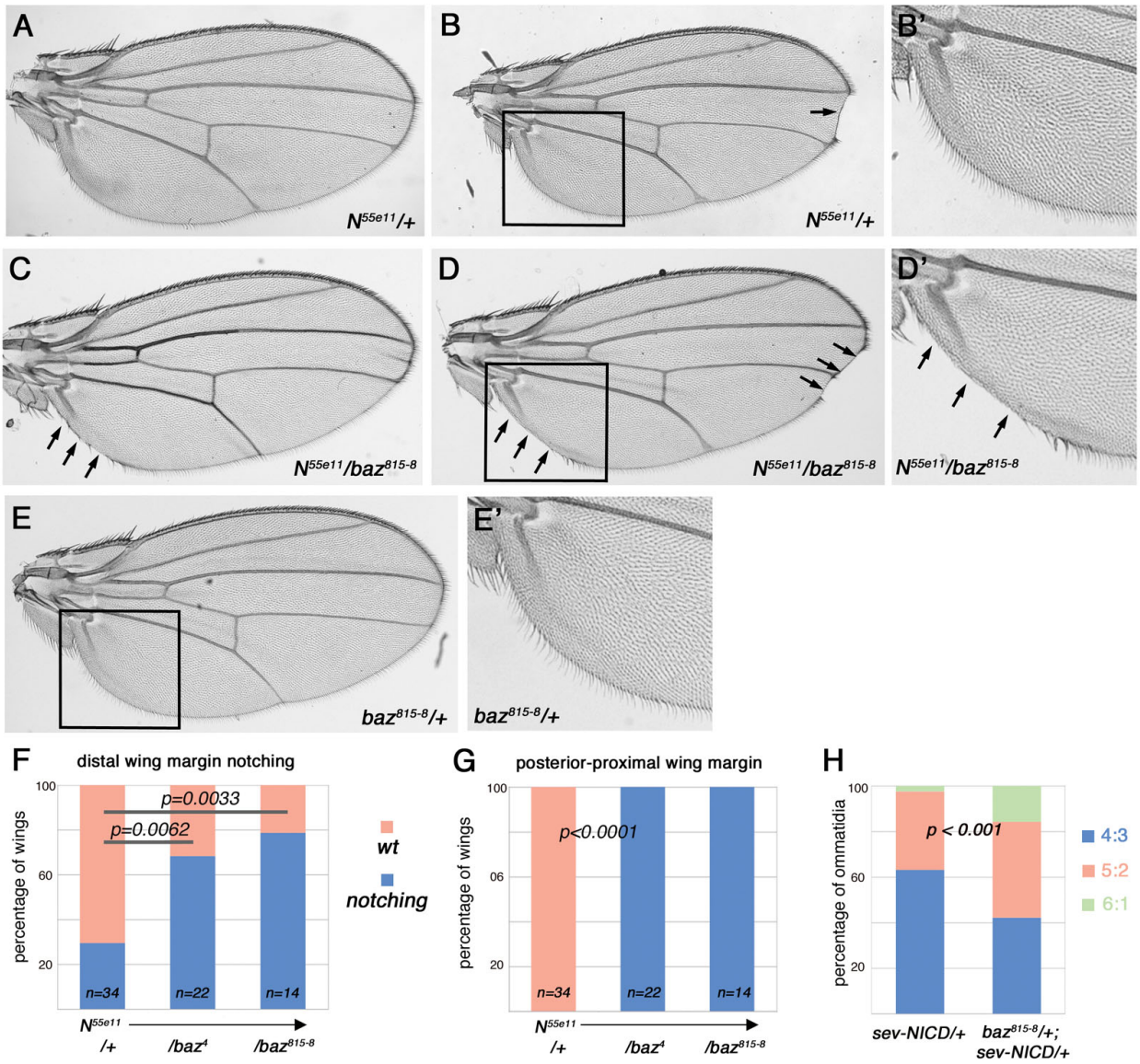

751

752

753

754 **Figure 3:**

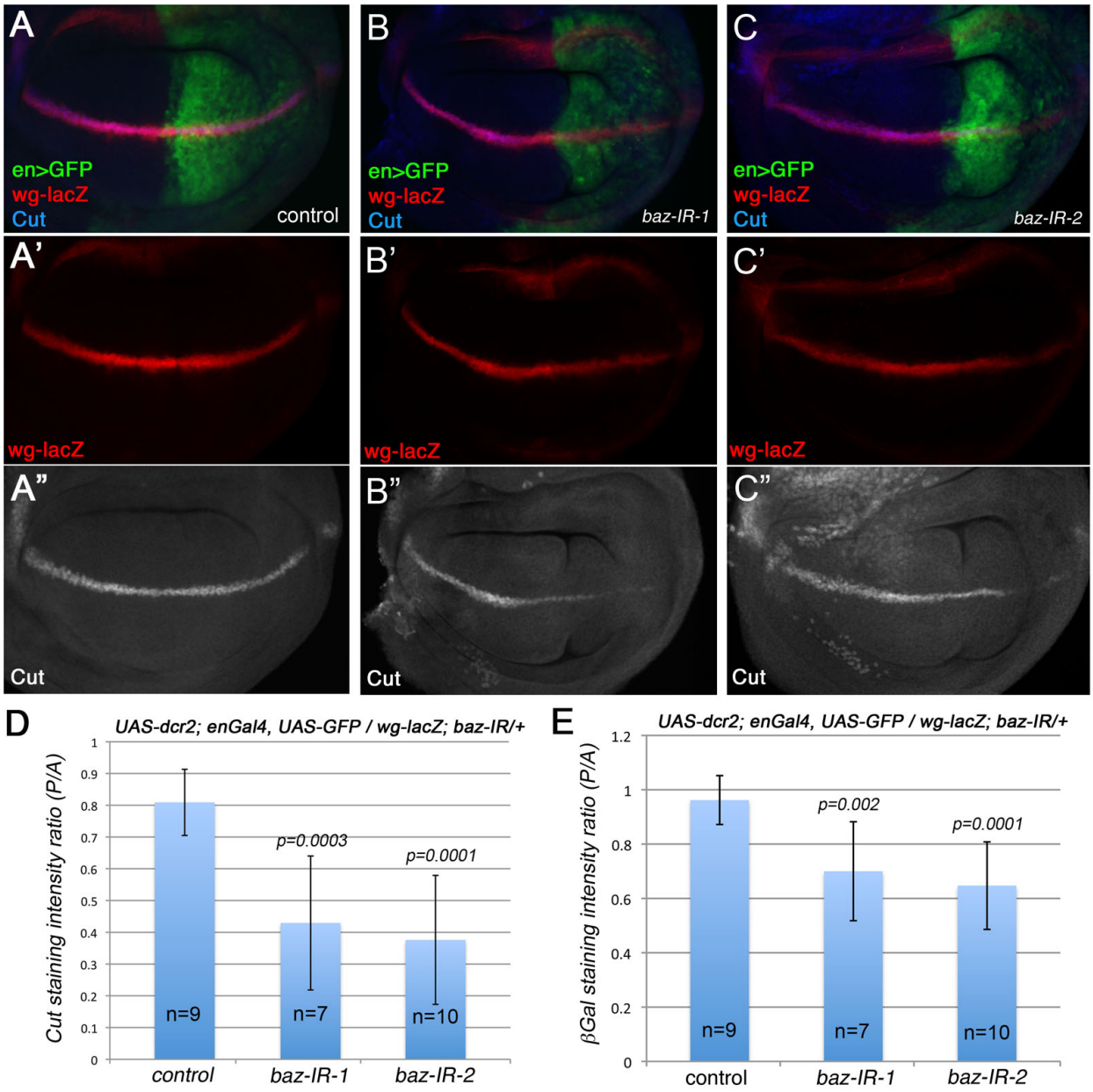

755

756

Figure 4:

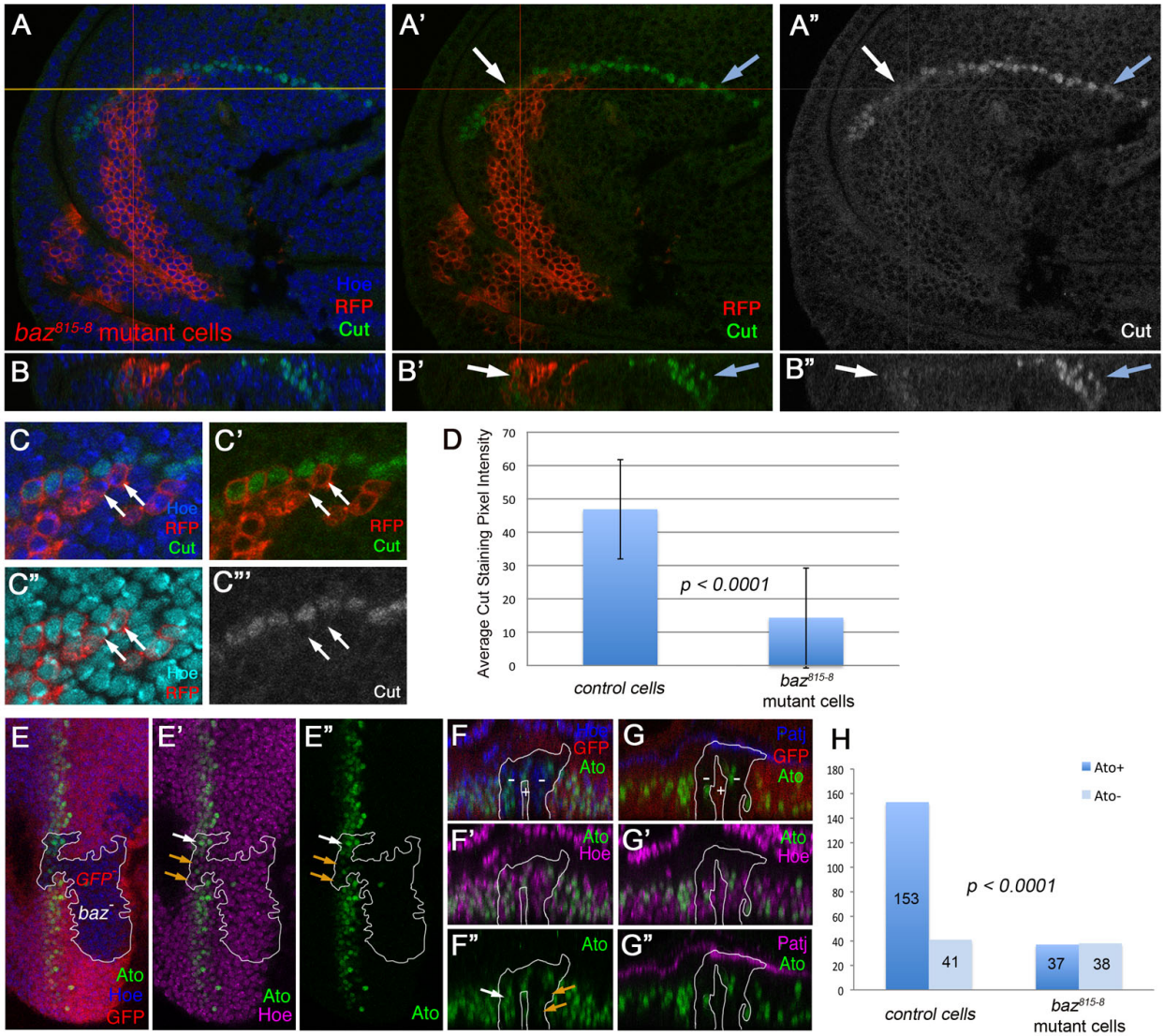
A
Hoe
RFP
Cut
baz815-8 mutant cells
A'
RFP
Cut
A"
Cut
B
B'
B"
C
Hoe
RFP
Cut
C'
RFP
Cut
C"
Hoe
RFP
C'''
Cut
D
Average Cut Staining Pixel Intensity
70
60
50
40
30
20
10
0
p < 0.0001
control cells
baz815-8
mutant cells
E
GFP
baz-
Ato
Hoe
GFP
E'
Ato
Hoe
E"
Ato
F
Hoe
GFP
Ato
F'
Ato
Hoe
F"
Ato
G
Patj
GFP
Ato
G'
Ato
Hoe
G"
Patj
Ato
H
Ato+
Ato-
180
160
140
120
100
80
60
40
20
0
153
41
37
38
p < 0.0001
control cells
baz815-8
mutant cells

760 **Figure 5:**

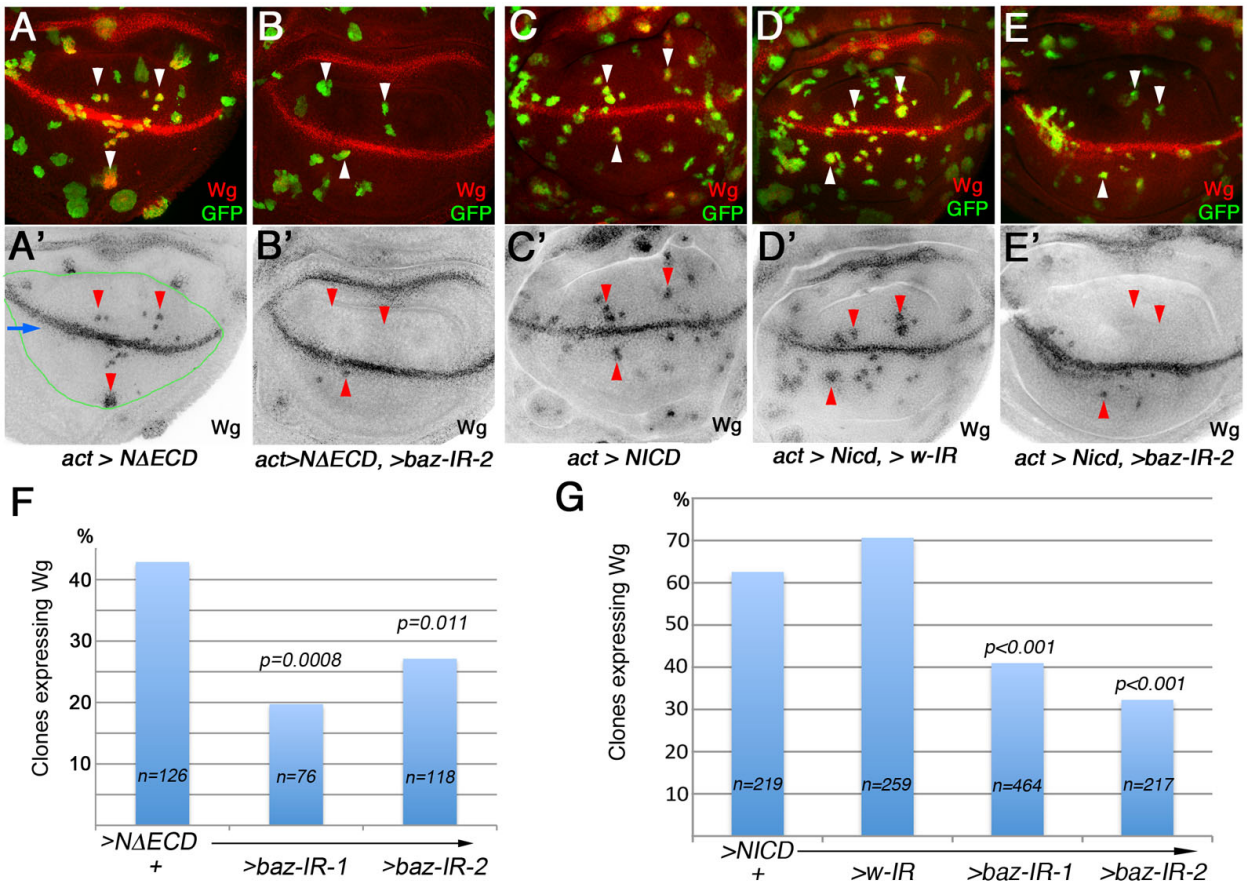

761

762

763 **Figure 6:**

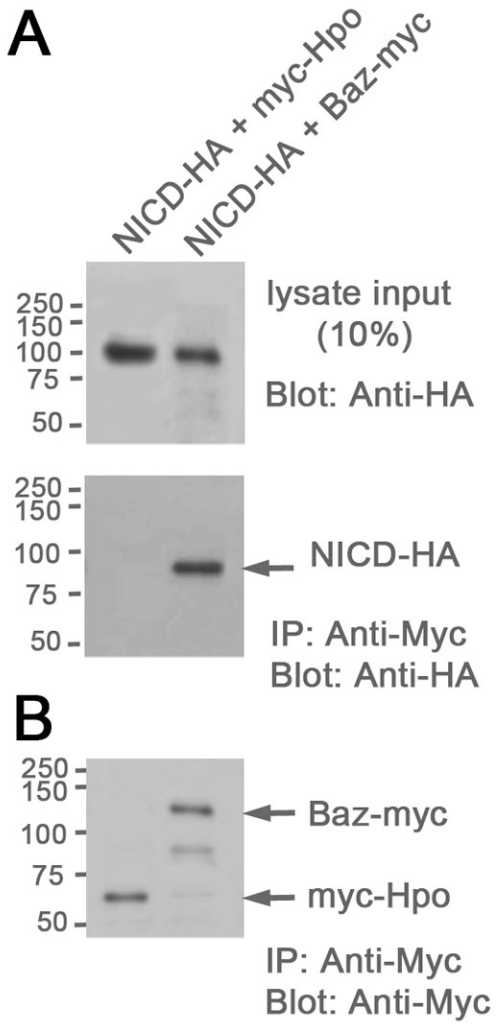

764